

Large-scale Shaking Table Test on Seismically Induced Failure of Earth-core Rockfill Dam

J. Liu, F.H. Liu & X.J. Kong

State Key Laboratory of Coastal & Offshore Engineering, Dalian University of Technology, Dalian, China

J. Liu, F.H. Liu & X.J. Kong

School of Hydraulic Engineering, Dalian University of Technology, Dalian, China



SUMMARY:

More and more high earth-core rockfill dams (ECRD) will be constructed in area with strong earthquakes. The failure mechanism of this type of dam during earthquake is still unclear, which limits engineers to accurately judge dam safety. In this paper, some new experimental technologies are developed and used to evaluate the seismic behaviours of ECRDs. They mainly include the pattern recognition system based on the Particle Image Velocimetry (PIV) technology to capture the deformations of the rockfills and the Fiber Bragg grating (FBG) sensors to monitor the strain of the earth-core. The test results show that the major effect of the simulated earthquake on the model dams is to cause sliding in both the upstream and downstream slopes while the earth-core can undergo large distortions without appreciable damage. The pattern recognition system provides an efficient tool to capture the particle movements of soil structures under shaking and the FBG sensor has the potentials to measure strain of low strength and low stiffness structures in shaking table tests.

Keywords: shaking table model test; earth-core rockfill dam; pattern recognition; Fiber Bragg grating sensor

1. INTRODUCTION

Over the last few decades, earth-core rockfill dams (ECRD) have been widely constructed and utilized around the world. More and more high-ECRDs are to be constructed in the southwest of China. These dams are mostly located in the high earthquake-intensity area. The failure mechanism of this type of dam during earthquake is still unclear.

Field observation is the most convenient method to investigate the dynamic damage of the ECRDs. However, only a limited number of dams have been damaged by earthquakes, particularly earthquakes of high magnitude (Iwashita, 2008). The lack of the practical data leaves us many unclear facts concerning the failure mode and failure mechanism caused by an extremely large earthquake. In addition, data from field observations can only be obtained before and after an earthquake; therefore, this type of data can only be used to study the failure characteristics of the structure, not the failure mechanism that occurs during the earthquake. Evaluations of seismic behaviour of dam have relied mostly on theoretical and numerical analyses. However, it is difficult to predict the deformation of the structure due to soil complexity in both the constitutive model and calculation parameters. The shaking table model test provides an effective method to research the failure mode and the failure mechanism of the rockfill dams under seismic loads due to its flexibility and convenience. It is also an important method to predict the deformation and the failure characteristics of high ECRD and verify the availabilities of the numerical methods. But few model tests have been performed till now.

Experimental research on the dynamic behaviour of the earth-rockfill dams mainly uses the 1g shaking table test and the dynamic centrifuge test. The centrifuge test can reproduce in-situ stress conditions, which is important to simulate the soil behaviour in a small-scale model, and this method has become a very useful tool to investigate the reliable behaviour of geotechnical system during earthquake loading (Kim, 2011). However, the model size used by this method is very small due to the limitation of the box's size and the vibration ability of the centrifuge, so the prototype's size simulated by this

method can not be very large and the measurement error is naturally enlarged. In addition, the present centrifuge can only afford one-dimensional test till now. The 1g shaking table test can not simulate the in-situ stress conditions, and this is the biggest limitation of this method. However, the performed 1g shaking table tests on rockfill dams have proved that the 1g shaking table test can represent the main failure characteristics of the rockfill dams, such as the base motion is magnified at the top of the model after it is transmitted through the dam body, the initial failure is local sliding of the rockfills near the crest, the natural frequency of the dam decreases with the increasing of the input motions, and so on. So the 1g shaking table test, despite its limitations associated with the centrifuge test, is still an effective method to investigate the seismic behaviour of the ECRDs.

Clough and Pirtz (1956) performed the first well-documented shaking table tests of rockfill dams. Based on model studies, they concluded that earth dams inherently are very resistant to earthquakes because of their flexible structure. The same shaking table was later used by Seed and Clough (1963) to study the earthquake resistance of sloping of core dams. They mentioned that the earthquake didn't produce a catastrophic failure of the models, its major effect being to cause some settlement of the upper section of the upstream slopes and a slight heaving in the lower sections of the slopes. These two studies established the basis for experimental study of ECRDs under earthquake. After that, some new shaking table tests about ECRD are studied (Baba and Nagai, 1987; Kim et al., 2011; Nakajima and Yamashita, 1970; Toshinori et al., 2008; Watanabe and Imaide, 1982). However, these studies mainly focused on the influence of the shaking on the frequency, the acceleration distribution of the dam body, the stability of the slopes and/or the deformation of the model. The failure of the earth-core was rarely studied.

There are two limitations in measurement technology in shaking table tests to investigate the failure mechanism of ECRDs. Firstly, it's not convenient to capture the deformation of granular materials such as rockfills. The coloured sand columns (Masukawa et al., 2004; Sabermahani et al., 2009; Torisu et al., 2010) and laser displacement sensors (Cihan et al., 2012) are traditionally used to observe the displacements of the dam body in shaking table tests. But the former can only show the deformed shape after test rather than the deforming process during test. The latter can only obtain the deformation of finite points. Secondly, the measurement of the strain of the model earth-core with low elastic modulus and low strength is always difficult. Electrical strain gauges are widely used in the strain measuring. However, electrical strain gauges are easily affected by electromagnetic interference with the shaking table. Further more, it is difficult to fix electrical strain gauges on the surface of the model earth-core.

In this paper, 1g shaking table tests are performed to evaluate the seismic behaviours of ECRDs. Some new experimental technologies are developed to monitor the dynamic response of the dam body. These technologies include: (a) a system for image collecting, fast storing and pattern recognition, in which 25 images with pixels of 4096*3072 are captured per second, total of 27 GB data can be stored during 90 seconds earthquake; and (b) application of specially designed distributed Fiber Bragg grating (FBG) sensors to measure the strain of the model earth-core which has low elastic modulus and strength. Different seismic waves are employed to investigate the failure mechanism of ECRDs.

2. EXPERIMENTAL TECHNOLOGIES

2.1. Pattern recognition system

Particle Image Velocimetry (PIV) technology (White et al., 2003; Liu et al., 2010), which has been widely used in soil tests in the last decade, provides a method to capture real-time displacement field of entire soil domain. However, previous PIV applications in soil tests were mainly limited to small scale models (small area to capture) under low speed conditions. While in the shaking table tests in this study, the soil domain is quite large (4 m×1.4 m) and the steel box (container of the model dam) was shaken with a high frequency (10 Hz). A camera with high pixel precision and high shot speed is required. Liu et al. (2010) tested three types of camera to capture images and presented measures to

improve the quality of the images in large scale shaking table model tests for sand slopes, which has similar model dimensions as that in this study. The results showed that the pixel precision was important for successful application of the PIV technology in shaking table model tests. If there are 158 pixels per 10 cm, the PIV analysis can effectively provide the deformation of the sand slope. However, the sampling frequency of the camera used by Liu (2010) is only 3.5 Hz, which is much lower than the exciting frequency (10 Hz). To obtain more abundant deforming information of the slopes, the sampling frequency should be improved and this will result in large amount of image data. Consequently, conflict occurs between storing such large amount of image data and the transmitting speed of the hard disk.

To deeply research the deformation mechanism of the soil structures, a system for image collecting, storing and pattern recognition is developed in this study. In this system, a high-speed, high-resolution camera is used to capture pictures. The frequency of the camera is 25 Hz, and the image resolution is 4096×3072. Thus, the data collection speed is approximately 300 MB/s. This is far beyond the maximum storage speed of normal hard disks. To store such large amount of data with the minimum cost, a specialized server machine with a large-capacity physical memory (32 GB) is linked to the camera. The large amount of image data are temporarily stored in the physical memory and then permanently written into the hard disk after experiments. Some rubber blankets are placed at the bottom of the tripod as a damping system to reduce the vibration's influence on the camera. The pattern recognition software is developed to analyze the deformation processes of specified regions.

2.2. FBG sensors

In recent years, FBG sensors have received considerable attention in optical sensing technology. These sensors are less affected by electromagnetic interference, have better accuracy, and can easily be embedded into the specimen. An FBG sensor is an optical interference pattern written by UV irradiation in the core of an optical fiber. If broadband light is coupled into the fiber, a narrow wavelength band is reflected. The peak wavelength of this reflection band, called Bragg wavelength λ_B depends on the period of the modulation of the refractive index along the fiber core Λ and the effective refractive index n_{eff} (Frieden, 2010):

$$\lambda_B = 2n_{\text{eff}}\Lambda. \quad (1)$$

If the grating is submitted to strain, the Bragg wavelength λ_B shifts by an amount $\Delta\lambda_B$. Under the condition of a uniform longitudinal strain along the optical fiber axis and no temperature changes (due to the short experimental time), the wavelength shift is related to the strain ε via the elastic-optical coefficient P_e :

$$\frac{\Delta\lambda_B}{\lambda_B} = (1 - P_e)\varepsilon. \quad (2)$$

Then the strain of the structure can be determined according to the test results of the wavelength shift.

In this study, distributed FBG strain sensors were designed to measure the strain of the model earth-core, as shown in Figure 1. The sensor consists of a fiber Bragg grating, two gripper tubes and two mounting supports, and the measurement accuracy is 0.5 μe . Based on the principle of friction and end-bearing piles, the mounting supports were designed to be a cube to increase its roughness of surface area in contact with clay and endure more external load. The fiber in both sides of the FBG is encapsulated with the two gripper tubes using epoxy resin. Since the FBG area is not in contact with epoxy resin, this type of FBG strain sensor can decrease the strain transferring loss and eliminate the multi-peaks phenomenon induced by the non-uniform bonding distribution of epoxy resin.

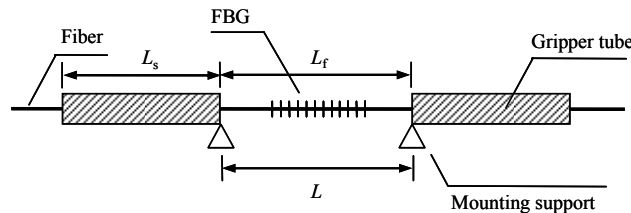


Figure 1. The schematic diagram of the FBG strain sensor

The strain of the gripper tube can be neglected in contrast with the strain of fiber. For a FBG sensor with central wavelength of 1550 nm, the relationship between the central wavelength shift of FBG $\Delta\lambda_B$ and the strain of the sensor ε can be written as

$$\Delta\lambda_{\text{FBG}} = \frac{1.2L}{L_f} \varepsilon . \quad (3)$$

The distance of the two mounting supports L of the FBG sensors used in this study is 10 mm, and the length of the fiber between the two gripper tubes L_f is also 10 mm, so the strain sensitivity of this type of FBG can be calculated to be 1.2 pm/ $\mu\varepsilon$ according to the formula (3).

The FBG sensor was fixed to a plastic beam with low elastic modulus to calibrate it and evaluate its strain transferring characteristic in the material with low elastic modulus. The test results showed that the deformation of this type of FBG sensor was coincident with the deformation of the bare FBG, and the coefficient of linear association is more than 0.9999. The experimental sensitivity of the FBG sensor was 1.1994 pm/ $\mu\varepsilon$ which was identical with the theoretical value. The results prove that this type FBG strain sensor works well on host materials with low elastic modulus (Ren, 2011)

3. TEST PROGRAM

3.1. Geometric Construction

Several 2D model tests are conducted to evaluate the seismic behaviours of ECRDs in empty-reservoir case. The model prototype is a typical ECRD with a height of 300 m. Based on the prototype's geometry size and the shaking table's practical ability, the model dam is 1m high and the crest is 0.1m width, the slope gradients are 1:1.9 and 1:1.8 in the upstream and downstream, respectively. So the length scale is 1:300 in this study. The height of the earth-core is 0.95 m and the widths are 0.05 m and 0.4 m in the top and bottom respectively. The elevation view of the cross-section of the model is shown in Figure 2.

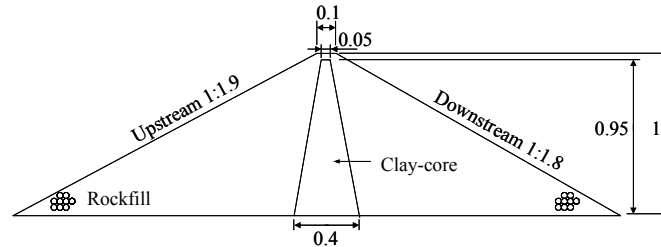


Figure 2. Elevation view of the cross-section of the model

The model is constructed in a rectangular steel box that is fixed on the shaking table using high-strength clamp bolts. The box is 4 m long and 1.5 m high with a Plexiglas-glazed front side that allows the model's failure process to be observed. The box's cross-section is trapezoidal (the width of the bottom is a little larger than the top) to decrease the soil pressure and reduce boundary effects.

3.2. Model Materials

3.2.1. Model rockfill material

Typically prototype rockfill materials are used to construct models on shaking tables so that the stress-strain behaviour and other mechanical properties of the model materials match those of the prototype materials. This method is typically used in some detailed analyses on the failure of soil structures (Clough and Pirtz, 1956; Iai, 1989; Lin et al., 2000; Meymand, 1988; Seed and Clough, 1963).

The prototype soil has an average dry unit weight of 2.1 g/cm³. The cohesion of this material is assumed to be negligible (Clough and Pirtz, 1956) and the internal friction angle is about 45°. According to the model and the steel box's dimensional limitations, the maximum grain size is

selected to be 20 mm. Different grading curves can be configured by different methods such as the similar particle distribution method, the equal quantity replacing method and the mixed method. Then relevant experimental tests are carried out to select a model material that can satisfy the requirements of gravity similitude law (Lin et al., 2000). The grading curves of the prototype material and the selected model material configured according to the mixed method are shown in Figure 3, and the mechanical properties of rockfill materials are listed in Table 1.

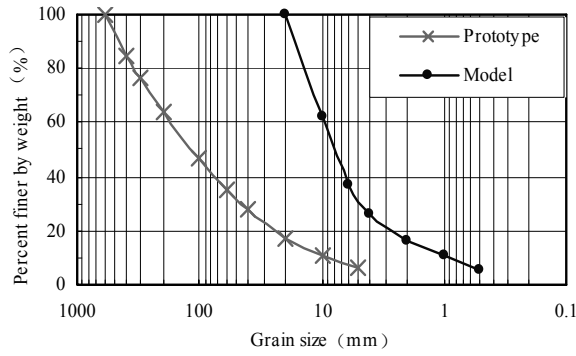


Figure 3. The grading curves of the prototype and model materials

Table 1. Mechanical properties of rockfill materials

Material	Max. dry density g/cm ³	Min. dry density g/cm ³	Selected density g/cm ³	Internal friction angle °
Model	1.929	1.572	1.85	46
Prototype	---	---	2.1	45

3.2.2. Model earth-core material

The prototype clay material is also selected as the model earth-core material to ensure the mechanical properties of the model materials are representative of the earthquake response of the prototype materials. Two model core materials marked ‘M1’ and ‘M2’ are configured in which the material ‘M1’ is clay material obtained from a construction site while ‘M2’ is constituted by mixing clay material and the standard sand with the same mass percent. Then the optimum water content test and the triaxial test are performed to obtain the mechanical properties of the selected materials, the test results are listed in Table 2. It can be seen that the density and internal friction angle of material ‘M2’ are closer to the prototype and the cohesion is lower than ‘M1’. These characteristics are required by the gravity similitude law (Lin et al., 2000). So material ‘M2’ is selected as the model earth-core material.

Table 2. Mechanical properties of earth-core materials

Material	Optimum water content %	Density g/cm ³	Cohesion kPa	Internal friction angle °
M ₁	24	1.81	16.3	20.6
M ₂	12	1.95	9.9	29.4
Prototype	---	2.1	35	31

3.3. Measurement System

The measurement system mainly includes the accelerometer, the camera and the FBG sensors. The schematic of the shaking table test with the measurement equipments are shown in Figure 4. Fourteen accelerometers were used to obtain the dynamic response of the model dam. The high-speed, high-resolution camera was placed in front of the model to capture the deformations of the model rockfills. Twelve FBG strain sensors were divided into two groups and each group contained six sensors to measure the vertical strain of the upstream and downstream earth-core slopes respectively, as shown in Figure 5. The six sensors in each side of the core were linked together by one fiber and the test results of these sensors could be recorded by a single channel to reduce the interference of the sensors to the structures.

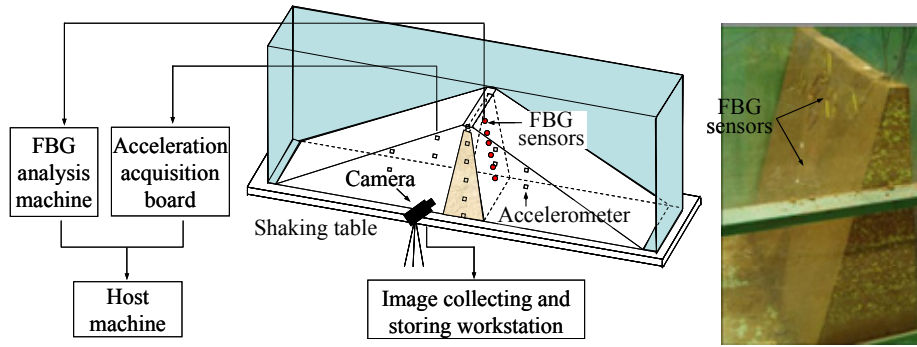


Figure 4. Schematic of the shaking table test with high shot speed cameras and FBG sensors

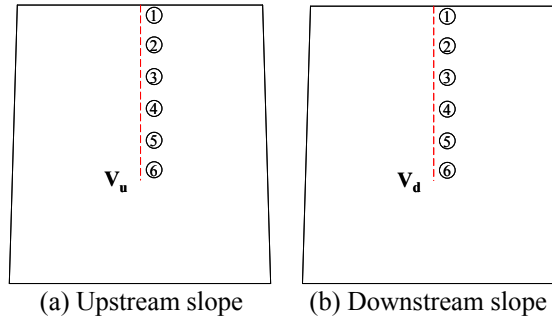


Figure 5. Distribution of the FBG sensors

3.4. Test Facilities and Input Motions

The model tests were carried on the shaking table in Dalian University of Technology. The dimensions of the shaking table are 3 m×4 m. The shaking table has a maximum acceleration of 1.0g and can utilize horizontal and vertical translation degrees of freedom, with the input frequency components ranging from 0.1 to 50 Hz.

Experiments were performed on three models with the same dimensions shown in Figure 2. Each model was shaken with different wave, as shown in Figure 6. Model 1 was shaken by a gradually increasing sinusoidal waveform with a frequency of 10 Hz and a 1/60 g/s amplification-increase ratio, as shown in Figure 6(a). The earthquake wave was applied to the bottom of the model horizontally until the slopes lost stability and large sliding occurred. Model 2 and Model 3 were shaken by waves artificially fitted according to the prototype's response spectrum, as shown in Figure 6(b). The duration time of the wave applied to Model 2 is 50 s while that applied to Model 3 is 20 s to compare the influence of the duration time of the earthquake waves on the damage of ECRDs. These two models were shaken by the horizontal and vertical waves synchronously in which the peak acceleration of the vertical wave was 2/3 times of the horizontal wave. Model 2 and Model 3 were subjected to seven level excitations with increasing magnitude, and the peak accelerations of the horizontal wave were 0.1g, 0.2g, 0.4g, 0.6g, 0.8g, 1.0g and 1.2g respectively.

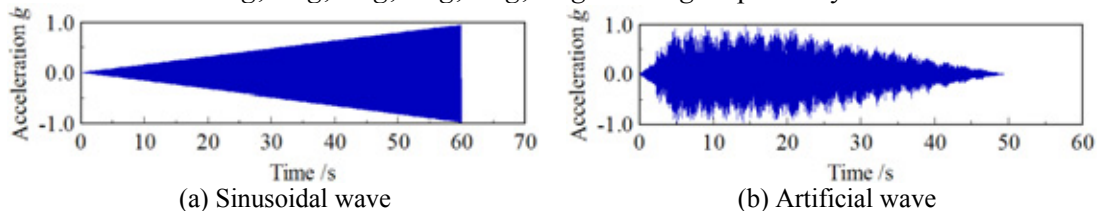


Figure 6. Input earthquake waves

4. TEST RESULTS

4.1. Acceleration response of the Dam Body

The acceleration distributions at the central axis of the model under different input accelerations are

shown in Figure 7. The dynamic response of the model is noticeably enlarged at top portion of the model, and the maximum amplification factor is about 2.5. It also can be seen that the amplification factor decreases with the increasing of the input accelerations. These results are consistent with the qualitative law of the rockfill dams under earthquake.

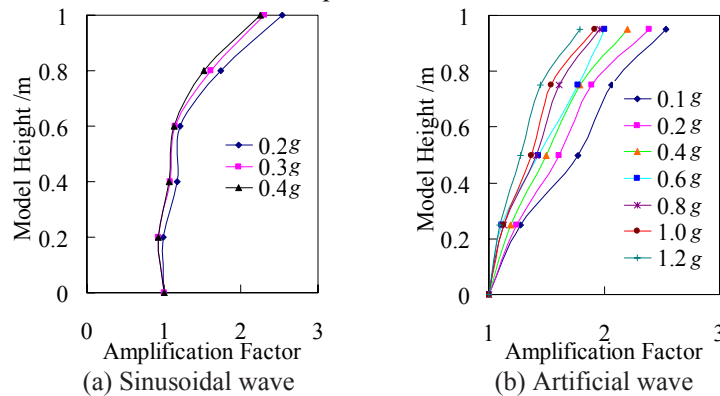


Figure 7. Distribution of the acceleration in the middle of the dam model

4.2. Failure Process of the Dam Body

The image collection and pattern recognition system monitors the deformation process until the model reaches failure. The vector lines in the following figures are obtained from PIV analysis. Their lengths and directions represent the observed points' displacements in the current picture relative to those in the previous picture, also known as the incremental displacement. Model 1 is chosen for the analysis of the dam's general failure process, which is described below.

The base motion is magnified at the top of the model after it is transmitted through the dam model. An early failure sign is found as the slope slides shallowly in the vicinity of the crest of the downstream (see Figure 8(a)) and subsequently slides in the upstream. As the excitement intensity increases, the quantity of sliding grains gradually increases, resulting in an expanding shallow failing zone in the downstream (Figure 8(b)) and upstream slopes. The sliding layer depth also gradually spreads to the inside of the model (Figure 8(c)). During the shaking, the core moves slightly and no obvious deformation occurs. Finally, the upper part of the core exposes out due to the sliding of the rockfills.

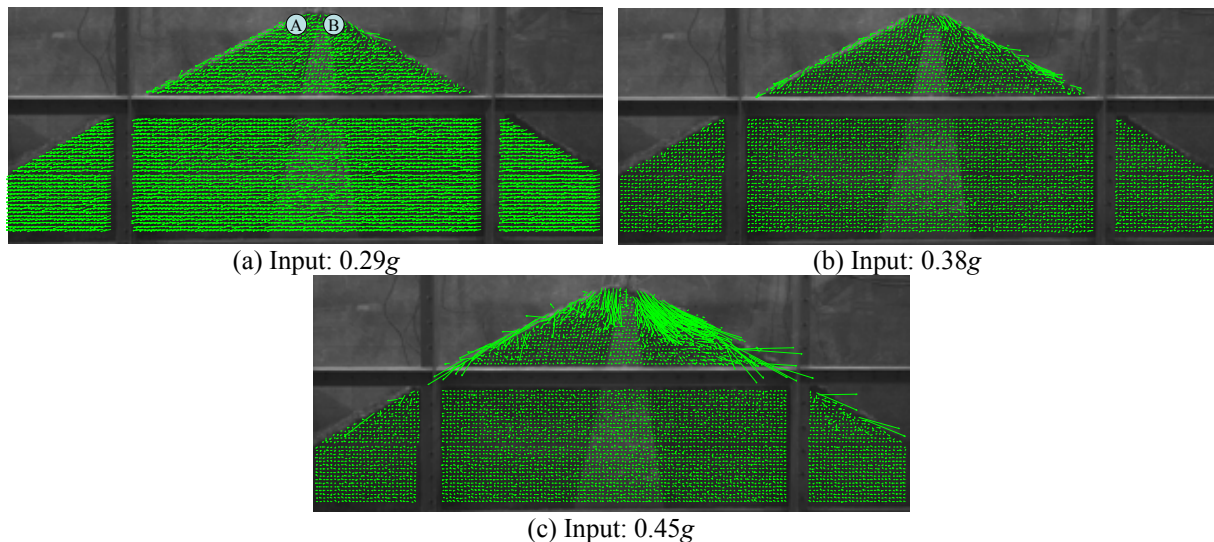


Figure 8. Failure process of the dam body

Figure 9 shows the real-time displacements of two observed points marked A and B in the upstream and the downstream slopes respectively, as shown in Figure 8(a). The total displacements of points A and B are almost identical when the input acceleration is small. With the increasing of the shaking, the total displacement of Point B is gradually larger than Point A. It clearly shows that the upstream slope

is much more stable than the downstream slope due to the steeper gradient of the downstream slope. The failure process of the dam body under artificial wave (Model 2, 3) is similar to that of the sinusoidal wave (Model 1). The relationship between the crest settlement rate δ (the ratio of the crest settlement to the model height) of each model and the peak acceleration is shown in Figure 10. It can be seen that the crest settlement results from the artificial wave is much lower than that from the sinusoidal wave under the same peak accelerations due to the differences of the energy inputting. It also can be seen that the earthquake duration time have large effect on the dam deformations, and the crest settlement of Model 2 is almost 2 times larger than that of Model 3. So we must consider the frequency, the peak acceleration and the duration time of the earthquake when evaluating the stability of the dams.

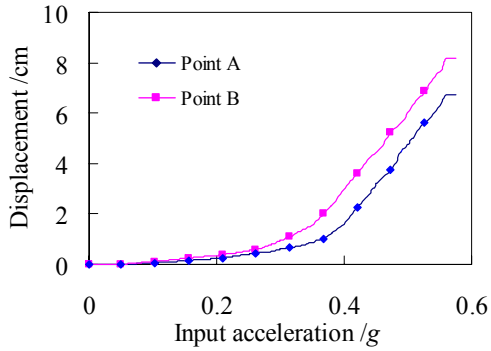


Figure 9. Total displacements of Points A and B

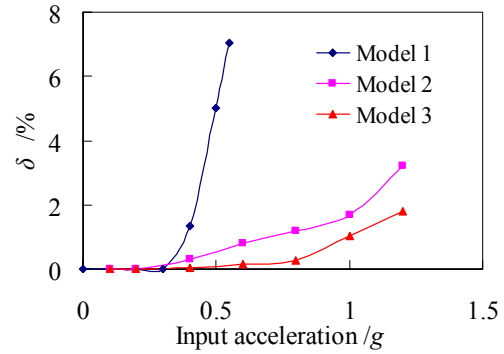


Figure 10. Crest settlements of each model

The inconsistent deformation between the rockfills and the earth-core is always a big problem to the ECRDs. Figure 11 shows the incremental shear strain in the interface between the rockfills and the earth-core of Model 1 in which the maximum value is filled by the red colour and the minimum value is filled by blue colour. It can be seen that large shear strains appear in the interfaces between the rockfills and the earth-core. The shear strains in both the upstream and downstream earth-core slopes are all firstly occur in top portion of the earth-core (see Figure 11a). As the increasing of the input motions, the rockfills further slid to the upstream and downstream slopes respectively. The regions with large shear strain in the interfaces also expanding constantly to the bottom of the earth-core.

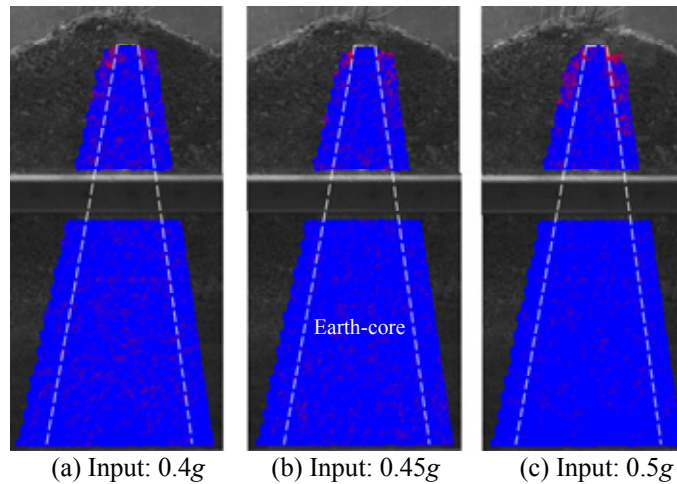


Figure 11. Contour of the shear strain in the interface (Model 1, Incremental shear strain)

4.3. Deformation and Stability of the Earth-core

4.3.1. Earth-core deformation of Model 1

The FBG sensors labeled '4' located in middle of the upstream and downstream respectively (as shown in Figure 5) are selected to analyze the deformation and stability of the earth-core. Figure 12 shows the strain time-history curves of these two sensors in which the positive value means tension while the negative value means compression. It can be seen that the strains of both the upstream side

and the downstream side increase gradually with the increasing of the input motion when the input acceleration is less than 0.4g. This phenomenon demonstrates that the earth-core is in elastic state. As the excitement intensity increases, the earth-core changes to plastic state and the tensile strain is greater than the compressive strain in the upstream side while the compressive strain is greater than the tensile strain in the downstream side. Finally, the upstream slope of the earth-core is in tensile state while the downstream side is in compressive state. These phenomena demonstrate that the earth-core deforms to the downstream direction.

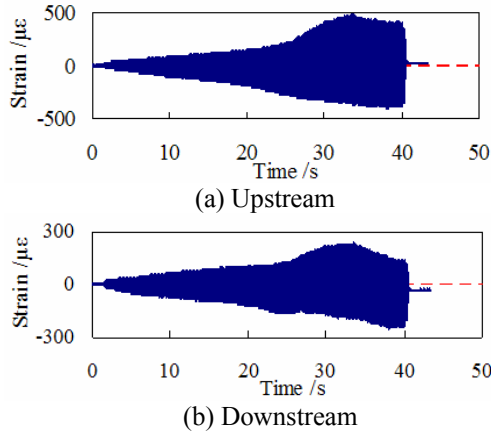


Figure 12. Strain time-history curves of the 4[#] vertical sensor of Model 1

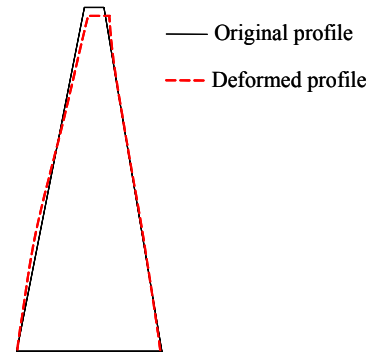
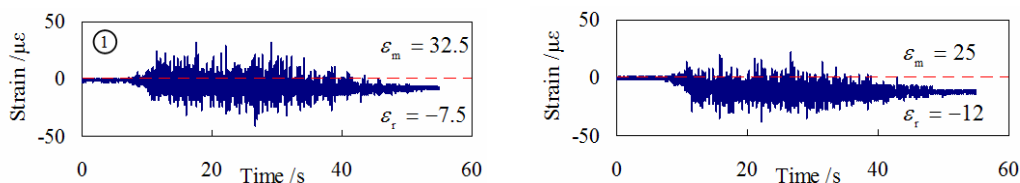


Figure 13. Deformation of the earth-core

As discussed above, the simplified deformation diagram of the earth-core is shown in Figure 13, i.e., the earth core deforms toward to the downstream direction and the settlement also occurs inevitably. It is mainly because that the downstream slope (with slope gradient 1:1.8) is steeper than the upstream slope (with slope gradient 1:1.9) and its stability is also lower than the upstream slope as discussed above. So the restraint of the rockfills to the earth-core reduced due to the sliding of the downstream rockfills, and then the earth-core easily deforms towards to the downstream direction under the combined actions of the inertia force and the driving force of the upstream rockfills.

4.3.2. Earth-core deformation of Model 2 and Model 3

In this section, the FBG sensors labelled ‘4’ are also selected to research the deformation and stability of the earth-core of Model 2 and Model 3. Figure 14 shows the strain time-history curves of the 4[#] vertical sensor of Model 2 during each level excitation. It can be seen that the strain wave shapes of this sensor during each load are approximate, so this type of strain sensor can be used to measure strain of low strength and low stiffness structures such as earth-core in shaking table tests effectively. The maximum tensile strain ε_m (the maximum value during each quake) and the residual strain ε_r (the difference between the strain after the shaking and the initial strain before shaking) monitored by the sensor of No. 4 during each load are also illustrated in Figure 14, and they are summarized in Figure 15. It can be seen that the maximum tensile strains of the vertical sensors present nearly linear relationship with the peak acceleration. So the earth-cores have good performances during the earthquake. From Figure 15(b) we can see that both upstream and downstream slopes of the earth-core are in compressive state during the first two level excitations due to the settlement of the earth-core. After the third level, the upstream slope transforms to be in tensile state and the tensile strain increases gradually with the increasing of the excitement intensity; however, the downstream slope is always in compressive state during the whole shaking. As discussed above, the deformation mode of the earth-core of Model 2 is the same as Model 1, i.e., the earth-core deforms toward to the downstream direction and the settlement also occurs (as shown in Figure 13).



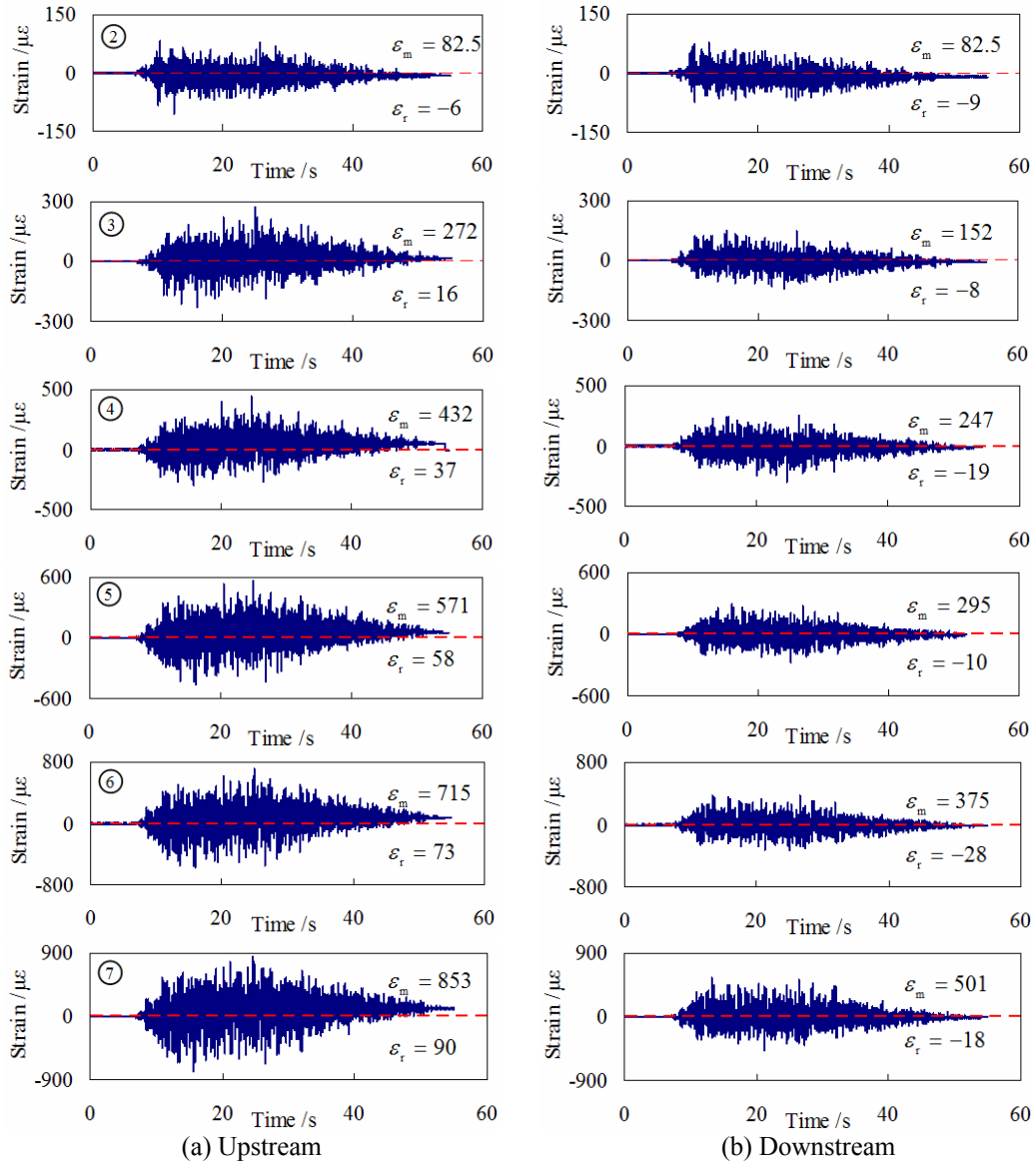


Figure 14. Strain time-history curves of the 4# vertical sensor of Model 2 during each load

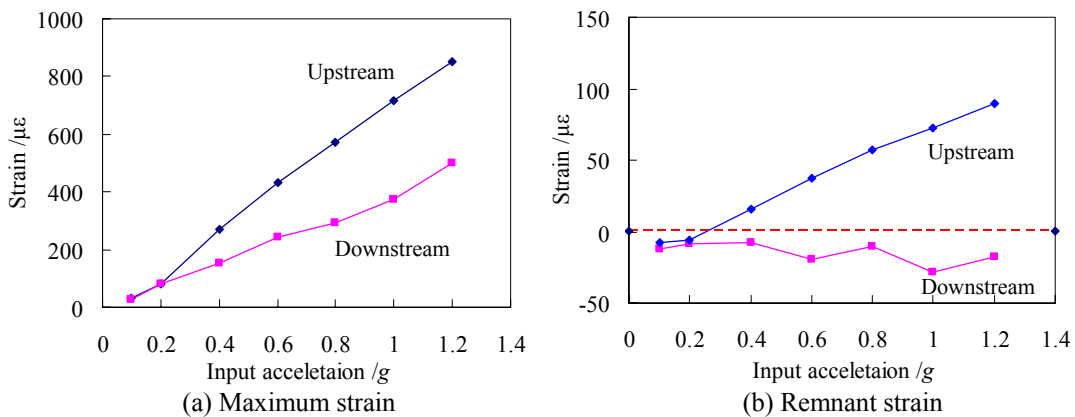


Figure 15. The maximum tensile strain and remnant strain of the 4# vertical sensor of Model 2 during each load

The deformation mode of the earth-core in Model 3 is the same as Model 2. However, the maximum tensile strain and the residual strain of Model 3 are smaller than Model 2 because the duration time of Model 3 (20 s) is shorter than that of Model 2 (50 s).

The laboratory ultimate tensile strain tests of several different prototype clay materials (Research Group on Prevention against Cracking of Earth Dams, 1973) and the in-situ test of clay materials (Li, 1992) all show that the ultimate tensile strain of the clay material is larger than $1000\mu\epsilon$. However, the maximum tensile strain and the remnant strain of the earth-core monitored by the FBG sensors in this study are all less than $1000\mu\epsilon$. So the earth-core is stable under the shaking used in this study.

As discussed above, the major effect of the simulated earthquake on the model dams is to cause sliding in both the upstream and downstream slopes, and the earth-core is naturally stable and can undergo large distortions without appreciable damage. The test results are consistent with the previous studies (Clough and Pirtz, 1956; Seed and Clough, 1963), so the test results are reasonable in this paper. The test results also reflect that the pattern recognition system can effectively capture the deformation mechanism of the discrete structures and the FBG strain sensors have potentials to measure strain of low strength and low stiffness structures in shaking table tests.

5. CONCLUSION

In this paper, some 1g shaking table model tests are performed to evaluate the seismic behaviours of ECRDs. Some new experimental technologies are developed to monitor the dynamic response of the dam body. The main conclusions can be drawn as follows:

- (1) The major effect of the simulated earthquake on the model dams is to cause sliding in both the upstream and downstream slopes. The earth-core is naturally stable and can undergo large distortions without appreciable damage.
- (2) The failure process of the dam body under artificial wave is similar to that of the sinusoidal wave. However, the crest settlement resulting from the artificial wave is much lower than that from the sinusoidal wave under the same peak accelerations. In addition, the earthquake duration has great effect on the dam deformations.
- (3) Relative sliding in the interface between the rockfills and the earth-core leads to large shear strain in the interface. The shear strain firstly occurs in top portion of the earth-core and then gradually extends to the bottom of it.
- (4) The test results in this paper are consistent with the qualitative law of the rockfill dams under earthquake, and these results can provide experimental data for validating the numerical model and the calculation theory.
- (5) The results of the model tests validate the effectiveness of the introduced experimental technologies. The pattern recognition system provides an efficient tool to capture the particle movements in shaking table tests of soil structures. The FBG sensor has potentials to measure low strength and low stiffness structures in shaking table tests.

ACKNOWLEDGEMENT

This work was funded by the National Natural Scientific Foundations of China (Grant No. 90815024, 51121005 and 50978045). These supports are gratefully acknowledged.

REFERENCES

- Baba, K. and Nagai, M. (1987). Dynamic failure test of model embankment. *International Symposium on Earthquake and Dams*, Vol 1, Beijing.
- Cihan, K., Yuksel, Y., Berilgen, M. And Cevik, E.O. (2012). Behavior of homogenous rubble mound breakwaters materials under cyclic loads. *Soil Dynamics and Earthquake Engineering* **34**,1-10.
- Clough, R.W., and Pirtz, D. (1956). Earthquake resistance of rockfill dams. *Soil Mechanics and Foundations Division* **82:2**,1-26.
- Frieden, J., Cugnoni, J., Botsis, J. et al. (2010). High-speed internal strain measurements in composite structures under dynamic load using embedded FBG sensors. *Composite Structures* **92:8**,1905-1912.
- Iai, S.(1989). Similitude for shaking table tests on soil-structure fluid model in 1-g gravitational field. *Soils and Foundation* **29:1**, 105-118.

- Iwashita, T. (2008). Elasto-plastic effective stress analysis of centrifugal shaking tests of a rockfill dam. The 14th World Conference on Earthquake Engineering, Beijing, China.
- Kim, M.K., Lee S.H., Choo Y.W. and Kim D.S. (2011). Seismic behaviors of earth-core and concrete-faced rockfill dams by dynamic centrifuge tests. *Soil Dynamics and Earthquake Engineering* **31**,1579-1593.
- Li, W.P., Yu, S.Z., Jiang, Z.Q., et al. (1992). Study on the engineering geological properties of the soil mass and the mining chink's forming conditions and its growth depth of the Huai River large dike. *Coal Geology & Exploration*, (2), 47-50. (in Chinese)
- Lin, G., Zhu, T. and Lin, B. (2000). Similarity technique for dynamic structural model test. *Journal of Dalian University of Technology* **40**:1, 1-8. (in Chinese)
- Liu, J., Liu, F. H., Kong, X. J. and Li, Y. S. (2010). Application of PIV in large-scale shaking table model tests. *Chinese Journal of Geotechnical Engineering* **32**:3, 368-374. (in Chinese).
- Masukawa, S., Yasunaka, M. and Kohgo, Y. (2004). Dynamic failure and deformations of dam models on shaking table tests. In: *Thirteenth World Conference on Earthquake Engineering 2004*; Vancouver, Canada, 2359-2371.
- Meymand, P.J.(1998). Shaking Table Scale Model Tests of Nonlinear Soil-Pile-Superstructure Interaction in Soft Clay. *PhD dissertation*; U.C. Berkeley.
- Nakajima, Y. and Yamashita, S. (1970). The new earthquake resistance design method of rockdill dams with impervious face. *Proc. , ICOLD IX, Montreal*.
- Ren, L., Zhang, Y., Li, D.S., Liu, J. et al. (2011). Application of FBG sensor in clay core wall dam structure model test. *Journal of Optoelectronics Laser*, **22**:8, 1124-29. (in Chinese)
- Research Group on Prevention against Cracking of Earth Dams (1973). Measurement of Tensile Characteristics of Cohesive Soils and Preliminary Investigation on Cracking of Earth and Rockfill Dams, *Journal of Tsinghua University(Science and Technology)*, (3), 61-71. (in Chinese)
- Sabermahani, M., Ghalandarzadeh, A. and Fakher, A. (2009). Experimental study on seismic deformation modes of reinforced-soil walls. *Geotextiles and Geomembranes* **27**,121-136.
- Seed, H. B., and Clough, R.W. (1963). Earthquake resistance of sloping core dams. *Journal of Soil Mechanics and Foundation division, ASCE*, **89**:1,209-242.
- Torisu, S.S., Sato, J., Towhata, I. and Honda, T. (2010). 1-G model tests and hollow cylindrical torsional shear experiments on seismic residual displacements of fill dams from the viewpoint of seismic performance-based design. *Soil Dynamics and Earthquake Engineering* **30**,423-437.
- Toshinori, K., Kazunori U., Tomohiro K., Koji W. and Yoshiyuki M. (2008). Dynamic behavior for lightweight spillway with geosynthetics on small earth dam. *Geotechnical Earthquake and Engineering and Soil Dynamics IV Congress 2008*.
- Watanabe, H. and Imaide, H. (1982). Effect of frequency on dynamic failure of rockfill dam models. *Proc. 6th Japan Earthquake Engineering Symposium*.
- White, D. J., Take, W. A. and Bolton, M. D. (2003). Soil deformation measurement using Particle Image Velocimetry (PIV) and photogrammetry. *Geotechnique* **53**:7, 619-631.